



Enhanced electrocatalytic production of H₂O₂ at Co-based air-diffusion cathodes for the photoelectro-Fenton treatment of bronopol



Zhihong Ye^a, Diego R.V. Guelfi^a, Garbiñe Álvarez^b, Francisco Alcaide^b, Enric Brillas^a, Ignasi Sirés^{a,*}

^a Laboratori d'Electroquímica dels Materials i del Medi Ambient, Departament de Química Física, Facultat de Química, Universitat de Barcelona, Martí i Franquès 1-11, 08028, Barcelona, Spain

^b CIDETEC, Paseo Miramón 196, 20014, Donostia-San Sebastián, Spain

ARTICLE INFO

Keywords:

Bronopol
H₂O₂ electrogeneration
Photoelectro-Fenton process
Pre-pilot plant
Wastewater treatment

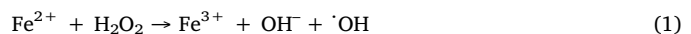
ABSTRACT

(Co, S, P)-decorated multiwalled carbon nanotubes (MWCNTs) have been synthesized following a hydrothermal route as electrocatalysts to manufacture large surface area air-diffusion cathodes with carbon cloth as substrate. The enhanced electrocatalytic H₂O₂ production as compared with Co-free MWCNTs cathodes was demonstrated in a 2.5-L pre-pilot plant with either a RuO₂-based or boron-doped diamond (BDD) anode, accumulating between 2- and 3-fold greater H₂O₂ contents with the catalyzed cathode. The good stability of this new material was ensured from the low Co leaching, with less than 9% Co released to solutions upon repeated usage. Aqueous solutions of the brominated organic preservative bronopol with 0.050 M Na₂SO₄ at pH 3.0 were comparatively treated by electro-oxidation (EO-H₂O₂), electro-Fenton (EF), UVA-assisted photoelectro-Fenton (PEF) and solar PEF (SPEF) at constant current density. SPEF with BDD anode and the catalyzed cathode showed the best performance, with total bronopol removal at 210 min and 94% mineralization after 360 min at 40 mA cm⁻², thanks to the action of ·OH, BDD(·OH) and sunlight. Formic acid was identified as main reaction by-product, whereas Br and N atoms were mainly converted to Br[·], BrO₃[·] and NO₃[·]. Some unidentified organic by-product containing Br and N was formed as well.

1. Introduction

H₂O₂ is one of the most versatile commodities with worldwide use in many end-use industries, including pulp and paper, custom synthesis and fine chemicals, textile, environmental, and others [1]. According to recent H₂O₂ market surveys, growth opportunities are clearly envisaged in the near future [2]. Within this framework, the electrochemical H₂O₂ production has emerged as an alternative to the classical anthraquinone method, since it prevents the use of toxic organic solvents needed in that synthesis as well as stabilizers that minimize its decomposition but are usually undesirable for many applications. Moreover, the explosion risks from storage and transportation of highly concentrated H₂O₂ solutions are reduced [3]. Off-site H₂O₂ electrogeneration finds an important application in advanced oxidation processes (AOPs) such as H₂O₂/UVC, H₂O₂/Fe²⁺ (UVA) and H₂O₂/O₃ for the removal of organic contaminants from wastewater [4,5]. Nonetheless, much progress has been made in recent years on the on-site environmental applications. In particular, the so-called Fenton-based electrochemical AOPs (EAOPs) like electro-Fenton (EF) and UVA or solar photoelectro-Fenton (PEF or

SPEF), are extremely effective to produce a powerful and clean oxidant like ·OH from Fenton's reaction (1) upon continuous and controlled H₂O₂ generation [6–8].



Traditionally, cheap carbonaceous materials like graphite [9], carbon felt [10–12] and reticulated vitreous carbon [11,13] have shown ability to produce H₂O₂ from the two-electron reduction of dissolved O₂ via reaction (2). However, much higher efficiency has been demonstrated upon atmospheric air supply: (i) through an air chamber that feeds a hydrophobized air-diffusion cathode [14–19] and (ii) to super-saturate the solutions with O₂ by means of a jet aerator [20] or high-pressure devices [21]. Some of these setups allow the fast accumulation of H₂O₂ with more than 90% current efficiency [18]. Significant advances have been achieved by the design of more efficient H₂O₂ electrolyzers [3] and the introduction of nanocarbons, either pristine or chemically modified, like carbon fibers [22], carbon nanotubes [23,24] or graphene [25–27], among others, because the increased electroactive surface area of the cathode enhances the O₂ mass

* Corresponding author.

E-mail address: i.sires@ub.edu (I. Sirés).

transport rate.



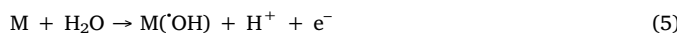
The EF treatment of organic pollutants employing an air-diffusion cathode has usually been carried out with pristine carbon, at either small [28] or pre-pilot scale [7,14,29–31]. This method leads to a fast removal of the parent pollutant at pH near 3.0 thanks to the action of ·OH formed in the bulk from Fenton's reaction (1), being much slower and usually incomplete the total organic carbon (TOC) abatement due to the accumulation of refractory complexes of Fe(III) with organic intermediates. The mineralization can be upgraded in PEF because UVA light photolyses most forms of Fe(III) via reactions (3) and (4), thus regenerating Fe²⁺ catalyst [6].



Some authors have attempted to increase the activity and selectivity of H₂O₂ production, reporting the positive contribution of Au-Pd and Pt-Hg nanoparticles [32]. For EF and PEF systems, a few articles discuss the modification of carbonaceous cathodes with non-ferrous metals and the study of their performance at small scale. For example, Pt-Pd nanoparticles were employed to decorate multiwall carbon nanotubes (MWCNTs) supported on reticulated vitreous carbon [33]. Other authors used metallic oxide nanoparticles like Ta₂O₅, WO_{2.72} or Ce_xA_{1-x}O₂ (A = Zr, Cu or Ni) immobilized on different substrates [34]. Nevertheless, the most promising and tested materials involve the modification of carbons with Co and Co-based catalysts. For example, CoS₂-based MWCNTs air-diffusion cathodes have been recently developed by our group to degrade the anaesthetic tetracaine [35], showing Co particles the best activity as compared to Cu, Ce, Mn or Fe-modified air-diffusion cathodes [36]. Barros et al. [37] prepared an air-diffusion cathode modified with Co(II) phthalocyanine for the EF treatment of the food dyes Amaranth. Unfortunately, stability tests are rarely addressed, but they are crucial to ensure the continuous reuse of cathodes.

The performance assessment of catalyzed cathodes under EF and PEF conditions has been pre-eminently carried out with small volumes of contaminated solutions. Therefore, there is a lack of information on Co-based carbonaceous air-diffusion cathodes at pilot scale. On the other hand, SPEF process constitutes a more viable alternative than PEF to scale-up the technology, since free sunlight replaces expensive UVA lamps yielding much quicker removals [7,14,18,38–42]. However, air-diffusion cathodes employed in SPEF were always uncatalyzed.

The combination of catalyzed carbonaceous cathodes with electrocatalytic anodes (M) that foster the production of heterogeneous hydroxyl radical from water oxidation via reaction (5) might enhance the performance of the aforementioned EAOPs, as well as that of electro-oxidation with H₂O₂ production (EO-H₂O₂) in the absence of dissolved iron catalyst [43–45]. Among such advanced anodes, boron-doped diamond (BDD) thin films exhibit an outstanding performance, usually better than dimensionally stable metal oxides as RuO₂.



In this work, the industrial preservative bronopol (2-bromo-2-nitropropane-1,3-diol, $M = 199.989 \text{ g mol}^{-1}$) has been selected as model organic pollutant to test the ability of new Co-based air-diffusion cathodes to generate H₂O₂. As an effective antiseptic, bronopol is ubiquitous in cosmetics, creams and lotions [46]. Lately, important concerns have arisen due to its potential to release formaldehyde, a human carcinogen [47]. On the other hand, aquaculture has grown in recent years thanks to support from European Commission, as a future alternative to decreasing seafood population. Within this context, bronopol is one of the few medicinal products authorized for sea farming in Europe [48]. As a result of their usage, bronopol has been detected even in Arctic environments [49], mainly due to the lack of advanced wastewater treatment facilities [50] as well as the stability of this pollutant

against hydrolysis and photolysis [51]. To date, only one article has attempted the treatment of small volumes of bronopol solutions by EF and PEF, using commercial uncatalyzed air-diffusion cathodes [52].

Here, MWCNTs decorated with Co-based catalyst in the form of sulfide, very efficient for H₂O₂ production at small scale [35], were prepared as a preliminary step for the subsequent manufacture of air-diffusion cathodes with carbon cloth as substrate. For the first time, this type of cathode has been used to electrogenerate H₂O₂ and treat an organic pollutant like bronopol in 0.050 M Na₂SO₄ at pH 3.0 by EO-H₂O₂, EF, PEF and SPEF using a pre-pilot plant. The experiments were performed with a filter-press flow cell equipped with catalyzed or uncatalyzed cathode and BDD or RuO₂-based anode. The effect of current density (j) and bronopol concentration on its decay kinetics, mineralization, current efficiency and energy consumption was examined, and final carboxylic acids and inorganic ions were quantified.

2. Materials and methods

2.1. Chemicals

Commercial MWCNTs were supplied by Cheap Tubes Inc. (OD < 8 nm, L 10–30 μm, COOH content 3.86 wt.%). Concentrated sulfuric and nitric acids, cobalt(II) chloride hexahydrate, sodium thiosulfate pentahydrate, sulfur and sodium hypophosphite monohydrate, from Scharlau and Sigma-Aldrich, were of reagent grade. Nafion® perfluorinated resin solution 5 wt.% was from Sigma-Aldrich and extra pure 2-propanol from Scharlau. Reagent grade sodium sulfate and iron (II) sulfate heptahydrate (> 98%) were purchased from VWR and Panreac, respectively. Bronopol (98%) was purchased from Sigma-Aldrich. Carboxylic acids and salts used for obtaining the calibration curves were of reagent grade from Merck and Panreac. Ultrapure water from a Millipore Milli-Q system (resistivity > 18.2 MΩ cm) was employed to prepare all the aqueous solutions. Other chemicals were of either HPLC or analytical grade.

2.2. Manufacture of catalysts and air-diffusion cathodes

2.2.1. Synthesis of catalysts

(Co, S, P)-decorated MWCNTs electrocatalysts (i.e., CoS_xP_y/MWCNTs) were synthesized in two steps. First, CoS₂/MWCNTs were prepared according to Dong et al. [53] by mixing appropriate amounts of CoCl₂·6H₂O, Na₂S₂O₃·5H₂O and S in a PTFE autoclave of 0.25 L capacity, keeping a molar proportion of 2:2:1, with enough quantity of MWCNTs to obtain ca. 50 wt.% of nominal Co:S:P in the final sample. About 80% of the total autoclave volume was filled with Milli-Q water and kept at 140 °C for 24 h. Once cooled down, the powder was filtered and washed repeatedly with ultrapure water, ethanol and carbon sulfide. The supported nanoparticles were dried in an air oven at 80 °C. The second step ensured the stabilization of this catalyst by impregnation with a phosphorus precursor followed by thermal treatment. For this, 280 mg of NaH₂PO₂·H₂O were mixed with 500 mg of fresh CoS₂/MWCNT catalyst, with an atomic ratio Co:S:P of 1:1:1, and treated at 400 °C for 1 h, under argon stream. The CoS_xP_y content in the final supported electrocatalyst was 55 wt.%, corresponding to 27 wt.% Co, 18 wt.% S and 10 wt.% P. For comparison, non-decorated MWCNTs were also used in this work.

2.2.2. Manufacture of air-diffusion electrodes

The spraying method was used to manufacture air-diffusion cathodes of 30 cm² (6 cm × 5 cm) active geometric area [54]. Unmodified or (Co, S, P)-decorated MWCNTs were ultrasonically dispersed in appropriate amounts of 2-propanol, ultrapure water and Nafion® dispersion to form an ink. This ink was sprayed several times onto a carbon cloth with a carbon microporous layer substrate employed as diffusion layer (BASF A7NCV2.1 ELAT® V2.1, thickness 350 μm), using an air-brush gun fed with pure N₂. The material was dried every time in an air

oven at 60 °C for 20 min. The catalyst loading in the $\text{CoS}_x\text{P}_y/\text{MWCNTs}$ air-diffusion electrode was 2.0 mg cm^{-2} and the Nafion® content was 30 wt.% (dry weight).

2.3. H_2O_2 electrogeneration and treatment of bronopol solutions by EAOPs

The pre-pilot plant employed in this study was designed and constructed by us, and a sketch is reported elsewhere [31]. The purpose-made undivided electrochemical filter-press reactor contained a manufactured air-diffusion cathode and either a BDD thin film on a Si wafer or a $\text{Ti}|\text{RuO}_2$ -based anode. The exposed electrode area was 20 cm^2 (5 cm × 4 cm) and the interelectrode gap was 1.2 cm. Continuous H_2O_2 generation from reaction (2) was ensured by embedding the back side of the cathode in a PVC air chamber fed with pumped air, keeping an overpressure of 8.6 kPa. Electrolyses were run at constant j provided by an N5746 A System DC power supply from Agilent Technologies, which also displayed the cell voltage (E_{cell} , see Table S1). In EO- H_2O_2 and EF, light irradiation was prevented by covering the plant with an opaque cloth. In PEF, the flow reactor outlet was connected to an annular glass photoreactor (640 mL of irradiated volume) to illuminate the solution with an Omnilux 27E 160-W UVA lamp ($\lambda_{\text{max}} = 360$ nm). In SPEF, the photoreactor was a 41°-tilted plane (600 mL of irradiated volume) to collect sunrays perpendicularly, and treatments were carried out in sunny days in August 2018, ensuring a constant UV irradiance (300–400 nm) of ca. 32 W cm^{-2} , as measured on a Kipp & Zonen CUV 5 radiometer.

H_2O_2 electrogeneration trials and bronopol treatments were made in 0.050 M Na_2SO_4 at pH 3.0, the optimum value for Fenton's reaction (1) [6]. In EF, PEF and SPEF, 0.50 mM of Fe^{2+} catalyst was chosen for sufficient $\cdot\text{OH}$ production, as was found in systems with air-diffusion cathodes [28,31]. The surface of each fresh cathode was activated by electrolyzing a 0.050 M Na_2SO_4 solution at pH 3.0 and 35 °C with a RuO_2 -based anode at 25 mA cm^{-2} . After three consecutive runs of 360 min each, reproducible H_2O_2 profiles were obtained. The good stability of the (Co, S, P)-catalyzed cathodes was assessed from Co leaching. All the experiments with catalyzed cathodes were carried out in duplicate with only two different pieces, one for electrogeneration trials and another one for bronopol treatments.

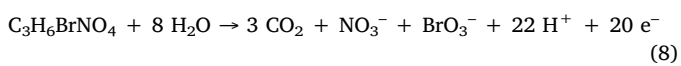
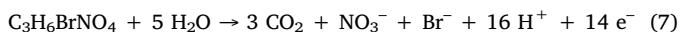
2.4. Apparatus and analytical methods

The pH of each solution was adjusted before current supply using a Crison 2000 pH-meter. The accumulated H_2O_2 was determined by the metavanadate method using a Shimadzu 1800 UV/Vis spectrophotometer at $\lambda = 450$ nm [55]. The current efficiency for H_2O_2 electrogeneration was calculated as proposed elsewhere [6].

The solution TOC was determined on a Shimadzu VCSN TOC analyzer after filtration with 0.45 μm Whatman PTFE filters. The mineralization current efficiency (MCE) upon treatment of V_s (L) at constant current I (A) during electrolysis time t (h) was then estimated as follows [6]:

$$\% \text{MCE} = \frac{n F V_s \Delta(\text{TOC})_{\text{exp}}}{4.32 \times 10^7 m I t} \times 100 \quad (6)$$

where F is the Faraday constant (96,487 C mol $^{-1}$), $\Delta(\text{TOC})_{\text{exp}}$ is the determined TOC removal (mg L^{-1}), 4.32×10^7 is a conversion factor and $m = 3$ is the number of carbon atoms of bronopol. Considering the pollutant mineralization to CO_2 , NO_3^- and Br^- (using the RuO_2 -based anode) or BrO_3^- (using BDD), as will be discussed below, the number n of electrons for the theoretical total mineralization was taken as 14 from Eq. (7) or 20 from Eq. (8):



The specific energy consumption per unit TOC mass (EC_{TOC} , kWh (TOC) $^{-1}$) during the same degradaiion trials was calculated from E_{cell} values as suggested elsewhere [6].

Bronopol concentration decay was monitored by reversed-phase high-performance liquid chromatography (HPLC) using a Waters 600 chromatograph, with a BDS Hypersil C18 6 μm (250 mm × 4.6 mm) column at 35 °C, coupled to a Waters 996 photodiode array at $\lambda = 211$ nm. The mobile phase was a 50:50 (v/v) acetonitrile/water (10 mM KH_2PO_4 at pH 3.0) mixture at 0.8 mL min^{-1} . All fresh samples were immediately diluted with acetonitrile to stop the degradation. The chromatograms displayed the peak of bronopol at retention time (t_r) of 4.2 min, with limits of quantification (LOQ) and detection (LOD) of 0.530 and 0.158 mg L^{-1} , respectively. Final carboxylic acids were quantified by ion-exclusion HPLC with the above liquid chromatograph, as reported in earlier work [41]. These chromatograms only displayed one peak associated with formic acid at $t_r = 13.9$ min.

Concentrations of BrO_3^- , Br^- and NO_3^- released during bronopol treatment were measured by ion chromatography [52]. Peaks were found at 2.3, 3.4 and 4.0 min, respectively. NH_4^+ content was measured according to the standard indophenol blue reaction [14]. The leached cobalt from catalyzed cathodes was determined by inductively coupled plasma-optical emission spectrometry (ICP-OES) on a Perkin Elmer Optima 3200 L spectrometer.

3. Results and discussion

3.1. H_2O_2 electrogeneration with catalyzed and uncatalyzed cathodes

Fig. 1a shows the H_2O_2 accumulation with time in the pre-pilot plant upon O_2 reduction on catalyzed and uncatalyzed cathodes at 40 mA cm^{-2} . The enhanced electrogeneration ability of the (Co, S, P)-decorated MWCNTs air-diffusion cathode was verified in all EAOPs tested, yielding 15.9, 7.4 and 3.5 mM H_2O_2 after 360 min of EO- H_2O_2 , EF and PEF, respectively, instead of 9.5, 4.7 and 0.9 mM achieved with the unmodified MWCNTs cathode. This is in agreement with the good results obtained with Co-based cathodes at smaller scale [36]. The lower accumulation in EF as compared to EO- H_2O_2 demonstrates the occurrence of Fenton's reaction (1) in the presence of 0.50 mM Fe^{2+} , thus ensuring a continuous source of $\cdot\text{OH}$. The conversion of H_2O_2 into $\cdot\text{OH}$ was accelerated in PEF, owing to the photoregeneration of Fe^{2+} under UVA irradiation, according to photo-Fenton reaction (3). Note that, in all cases, the profiles tended to reach a plateau, which resulted from the use of an undivided filter-press cell, where H_2O_2 was partially oxidized at the RuO_2 anode. Upon prolonged electrolysis, the decomposition rate tended to equate its electrogeneration rate at the catalyzed air-diffusion cathode [6].

The effect of j on H_2O_2 concentration was assessed for the three EAOPs under the same electrolytic conditions reported in Fig. 1a. As shown in Fig. 1b, the H_2O_2 accumulated at 360 min decreased to 11.3 and 4.0 mM in EO- H_2O_2 process at j of 25 and 10 mA cm^{-2} , respectively. This trend was expected since feeding of reagents required for reaction (2) is ensured and hence, the H_2O_2 production was uniquely dependent on the electron supply and can be effectively dosed by simply modulating the input current. However, Fig. 1c shows that the efficiency at 30 min decreased in the sequence 100% > 85% > 72%, when j was raised from 10 to 40 mA cm^{-2} . At the lowest j , O_2 was only reduced to H_2O_2 , whereas the competitive four-electron reduction to H_2O occurred to a gradually larger extent at a higher j , due to the change of the cathode potential to more negative values. As seen in Fig. 1c, the current efficiency underwent a progressive decay, which is not surprising because of the simultaneous oxidation of H_2O_2 at the anode surface and its cathodic reduction, as well as its chemical decomposition in the bulk. These destruction reactions justify that, at 360 min, a similar efficiency of 51–54% was obtained at all j values.

A similar effect of j on the time course of H_2O_2 was observed in EF (Fig. S1b) processes. Note that, in both systems, the increase of j

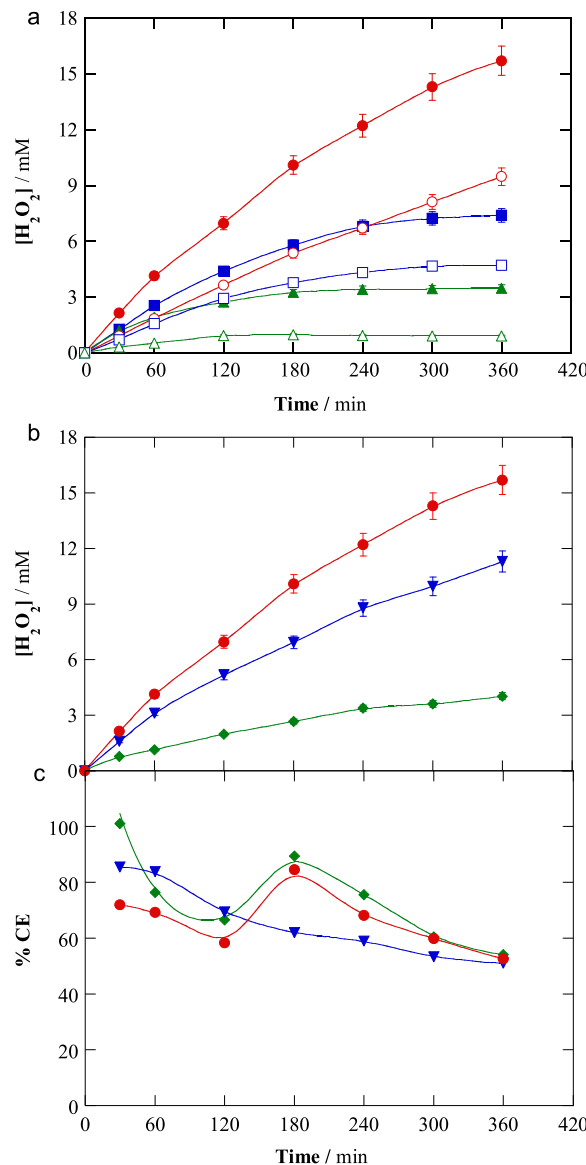


Fig. 1. (a) Time course of H_2O_2 concentration accumulated in 2.5 L of 0.050 M Na_2SO_4 at pH 3.0 and 35 °C using a filter-press reactor with a RuO₂-based anode and: (●, ■, ▲) (Co, S, P)-modified and (○, □, △) uncatalyzed MWCNTs air-diffusion cathodes. EAOP: (●, ○) EO- H_2O_2 , (■, □) EF with 0.50 mM Fe^{2+} and (▲, △) PEF with 0.50 mM Fe^{2+} and 160-W UVA lamp. Current density (j) of 40 mA cm^{-2} and liquid flow rate of 180 L h^{-1} . (b) Accumulated H_2O_2 concentration vs. electrolysis time under the above EO- H_2O_2 conditions using a (Co, S, P)-modified air-diffusion cathode at j : (◆) 10 mA cm^{-2} , (▼) 25 mA cm^{-2} and (●) 40 mA cm^{-2} . (c) Current efficiency during trials shown in plot b.

stimulated all aforementioned parasitic reactions, and also accelerated the Fe^{2+} regeneration from Fe^{3+} reduction at the cathode, thus favoring the H_2O_2 consumption by Fenton's reaction (1). However, the inherent upgrade in H_2O_2 electrogeneration at 25 and 40 mA cm^{-2} counteracted all these side reactions, eventually ending in a greater H_2O_2 accumulation in the order: 10 < 25 < 40 mA cm^{-2} .

The electrogeneration performance of the catalyzed and uncatalyzed cathodes was also compared using an undivided electrochemical reactor equipped with a BDD anode. Fig. S2 shows that under PEF conditions at 40 mA cm^{-2} , a much greater H_2O_2 accumulation was achieved again for the Co-based air-diffusion electrode, reaching 3.5 mM instead of 0.6 mM. Note that there was no difference in H_2O_2 accumulation between the RuO₂/air-diffusion (Fig. 1a) and BDD/air-diffusion cells, which means that in Fenton-based processes, the H_2O_2

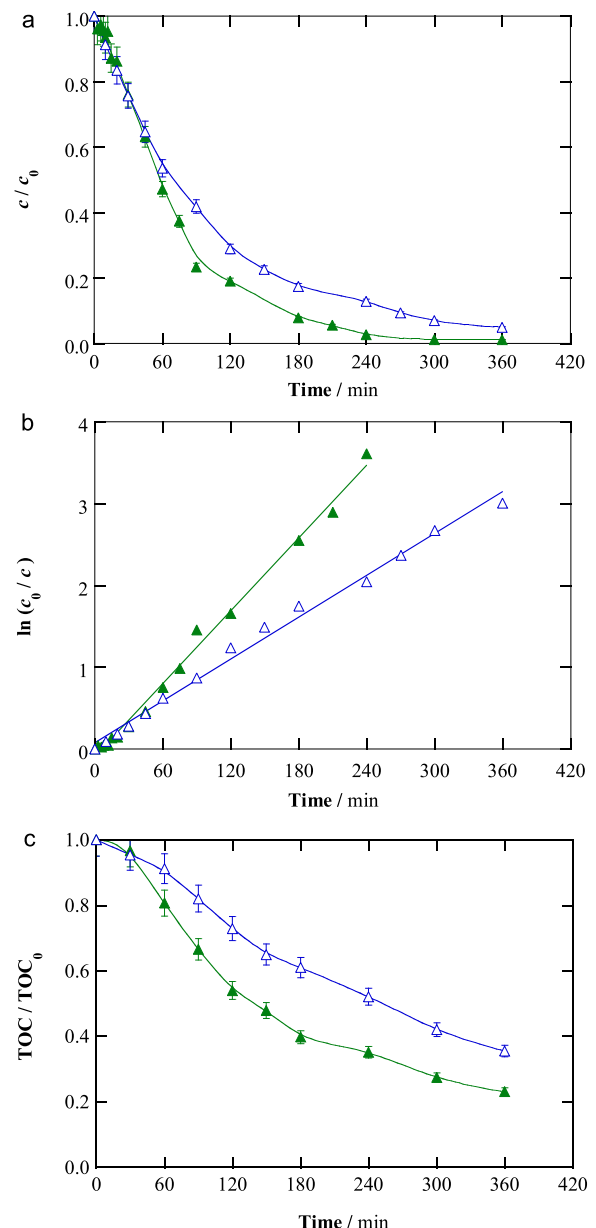


Fig. 2. Normalized (a) bronopol concentration and (c) TOC decays with electrolysis time during the PEF treatment of 2.5 L of 0.28 mM bronopol (10 mg L^{-1} TOC) solutions in 0.050 M Na_2SO_4 with 0.50 mM Fe^{2+} at pH 3.0 and 35 °C using a filter-press reactor with a RuO₂-based anode and (▲) (Co, S, P)-modified or (△) uncatalyzed MWCNTs air-diffusion cathode at j = 40 mA cm^{-2} and liquid flow rate of 180 L h^{-1} . (b) Pseudo-first-order kinetic analysis for data of plot (a).

was mainly destroyed via Fenton's reaction (1), which was predominant over its anodic destruction.

The stability of the (Co, S, P)-decorated MWCNTs air-diffusion cathodes with a large surface area (20 cm^2 in contact with the solution) is a crucial feature for their further implementation. This was assessed by monitoring Co leaching during the activation of fresh catalyzed cathodes, which revealed the accumulation of 0.68–0.99 mg L^{-1} during the first run, yielding undetectable traces below LOD (0.02 mg L^{-1}) in successive electrogeneration trials. Considering the catalyst composition and loading (Sections 2.2.1 and 2.2.2), 10.8 mg Co were exposed to the solution during the first activation, with a Co loose of 9% as maximal. On the other hand, Fig. S3 shows the images of the catalyzed cathode before and after activation under PEF conditions, using either a RuO₂-based or BDD anode. It can be observed that the central region,

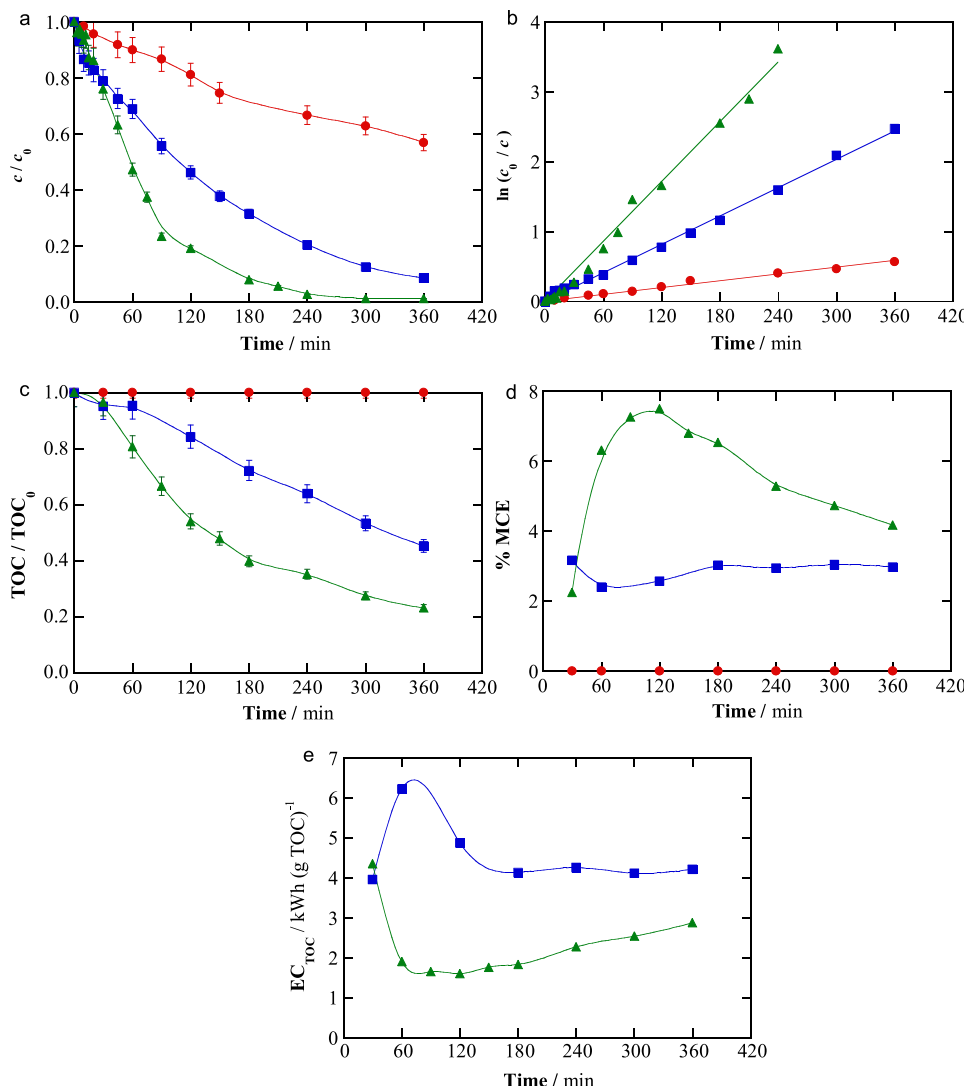


Fig. 3. (a) Normalized bronopol concentration removal vs. time and (b) corresponding pseudo-first-order kinetic analysis, (c) normalized TOC decay with electrolysis time and corresponding (d) mineralization current efficiency and (e) specific energy consumption per unit TOC mass during the treatment of 2.5 L of 0.28 mM bronopol solutions with 0.050 M Na₂SO₄ at pH 3.0 and 35 °C by (●) EO-H₂O₂, (■) EF with 0.50 mM Fe²⁺ and (▲) PEF with 0.50 mM Fe²⁺ employing a RuO₂-based anode and (Co, S, P)-modified MWCNTs air-diffusion cathode at $j = 40 \text{ mA cm}^{-2}$ and liquid flow rate of 180 L h⁻¹.

which contained the electrocatalytic coating, maintained its complete uniformity, with only some additional Fe(OH)₃ deposition, as typically occurs during Fenton-based electrochemical treatments. The large stability of the cathode allowed a good reproducibility upon successive trials, losing less than 1% efficiency after more than 20 electro-generation runs.

3.2. Treatment of bronopol solutions by EAOPs

Fig. 2a shows the decay of bronopol content during PEF treatment of solutions with 0.28 mM (10 mg L⁻¹ TOC) using a RuO₂-based anode at 40 mA cm⁻². It was completely removed after 360 min employing the catalyzed cathode, whereas 5% of pollutant was still present using the uncatalyzed cathode. This different behavior confirms that the higher H₂O₂ accumulation shown in Fig. 1a using the former cathode leads to a faster generation of 'OH from Fenton's reaction (1). Worth mentioning, bronopol was much more resistant than aromatic organic pollutants degraded by PEF at pre-pilot scale, whose complete removal is typically achieved in only few minutes. For example, less than 18 min were required to remove 0.174 mM naproxen at 50 mA cm⁻² under similar conditions [30].

In both PEF systems, bronopol concentration decay obeyed a pseudo-first-order kinetics (Fig. 2b), which is coherent with the generation of a constant amount of reactive 'OH as the main oxidant species. As expected, a significantly greater rate constant (k_{app}) resulted

from the electrolysis with the catalyzed cathode, i.e., 0.015 vs 0.009 min⁻¹. The mineralization of the same bronopol solutions followed the same trend, with Fig. 2c revealing a higher TOC removal (77% vs 64% at 360 min) when the electrochemical reactor was equipped with the Co-based cathode.

The performance of the catalyzed air-diffusion cathode under PEF conditions was compared with that observed in EO-H₂O₂ and EF. As shown in Fig. 3a, bronopol removal at 360 min was 44%, 92% and 100% in EO-H₂O₂, EF and PEF. All the decays agreed with a pseudo-first-order reaction kinetics, as highlighted in Fig. 3b, yielding k_{app} values of 0.002, 0.007 and 0.014 min⁻¹, respectively ($R^2 > 0.98$). The superiority of EF and PEF over EO-H₂O₂ arises from the abundance of 'OH produced in the bulk from Fenton's reaction (1), which are much more effective than both, direct anodic oxidation on the anode surface and mediated oxidation by RuO₂('OH). PEF was the most powerful treatment thanks to the continuous Fe²⁺ regeneration from reaction (3), which resulted in a larger production of 'OH during the run. Note that this effect has been rarely observed during the treatment of less refractory pollutants, since the photolytic action of UVA light requires long reaction times that are not commonly needed by aromatic molecules, in contrast to the current aliphatic contaminant.

TOC removal during the application of the same three EAOPs is depicted in Fig. 3c. No mineralization was achieved in EO-H₂O₂, thus confirming the small oxidation power of RuO₂('OH). In contrast, up to 52% TOC abatement was attained after 360 min of EF, which resulted

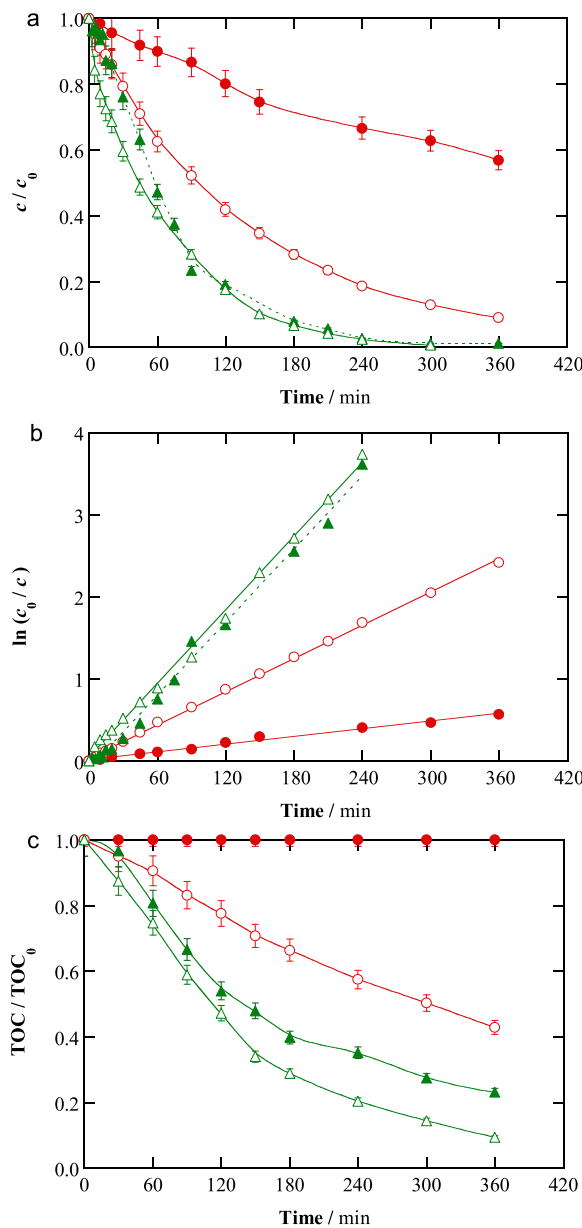


Fig. 4. (a) Normalized bronopol concentration removal with time, (b) corresponding pseudo-first-order kinetic analysis and (c) normalized TOC decay with time during the (●, ○) EO-H₂O₂ and (▲, △) PEF treatments of 0.28 mM bronopol solutions under the same conditions of Fig. 3 using a (●, ▲) RuO₂-based or (○, △) BDD anode and (Co, S, P)-modified MWCNTs air-diffusion cathode.

from the progressive combustion of many degradation by-products by 'OH. However, many of them became quite refractory and could only undergo a slow destruction upon irradiation with UVA light, which photodecomposed some of the complexes formed between Fe(III) and organic aliphatic by-products. The slow and only partial TOC removal yielded a very low MCE, always below 8%. The highest mineralization current efficiency along with the corresponding lowest EC_{TOC}, calculated from cell voltage values given in Table S1, were found for PEF treatment (Fig. 3d and e).

The effect of j on the performance of PEF treatment with the RuO₂-based anode and catalyzed cathode can be seen in Fig. S4. As expected from the lower H₂O₂ accumulation (Fig. S1b), bronopol removal was slower at 25 mA cm⁻² (96%) and 10 mA cm⁻² (85%) as compared to PEF at 40 mA cm⁻², yielding k_{app} values of 0.010 and 0.005 min⁻¹ (R^2

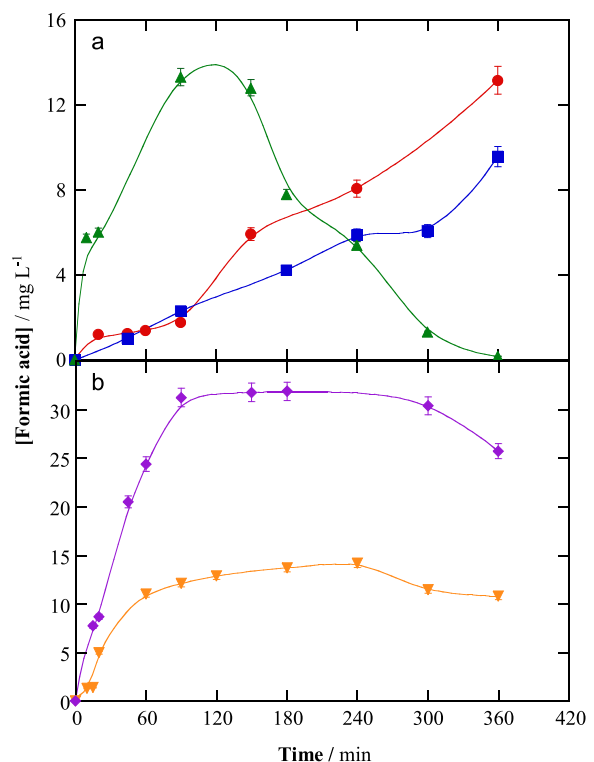


Fig. 5. (a) Time course of formic acid formed during the (●) EO-H₂O₂, (■) EF and (▲) PEF treatments of the 0.28 mM bronopol (10 mg L⁻¹ TOC) solutions shown in Fig. 3. (b) Formic acid accumulation profiles during the PEF treatment under the conditions shown in plot (a), at: (▼) 0.56 mM (20 mg L⁻¹ TOC) and (◆) 0.84 mM (30 mg L⁻¹ TOC) bronopol.

≥ 0.99). Similarly, smaller TOC decays (72% and 56%, respectively) were attained. However, gradually higher MCE and lower energy consumption values resulted when j decreased from 40 to 10 mA cm⁻², which can be explained by the excessive number of parasitic reactions that appear as the applied current is increased [6,8].

The effect of initial bronopol concentration on the same PEF treatment at 40 mA cm⁻² was also investigated, trying to assess the feasibility of treating highly polluted solutions by the most powerful EAOP. In Fig. S5a, trials with 0.28, 0.56 and 0.84 mM bronopol are compared. Total degradation was not possible for solutions with > 0.28 mM, attaining removals of 88% as maximum at 360 min. The decays still obeyed a pseudo-first-order kinetics, although with smaller k_{app} values of 0.006 min⁻¹. This deceleration at too high pollutant contents was confirmed from the time course of TOC (Fig. S5c), which was removed by 52% and 44% for 0.56 and 0.84 mM bronopol, thus suggesting that the number of accumulated 'OH at 40 mA cm⁻² was insufficient to reach a faster mineralization. Typically, the presence of a large amount of organic matter enhances the MCE of EAOPs, owing to the minimization of parasitic reactions involving the 'OH. However, the slow TOC removal at high bronopol concentration prevented obtaining high MCE values (Fig. S5d). Similarly, lower energy consumptions per unit TOC mass, as compared to PEF at 40 mA cm⁻², could not be attained (Fig. S5e).

Aiming to enhance the performance of PEF treatment with the catalyzed cathode at 40 mA cm⁻², the RuO₂-based anode was replaced by BDD. The influence of the anode nature was dramatic in EO-H₂O₂ since it yielded bronopol and TOC removals of 91% (Fig. 4a) and 58% (Fig. 4c) at 360 min using BDD instead of 44% and 0% reached with RuO₂-based anode. These results arise from the high oxidation power of BDD('OH), which was accumulated with a constant concentration that

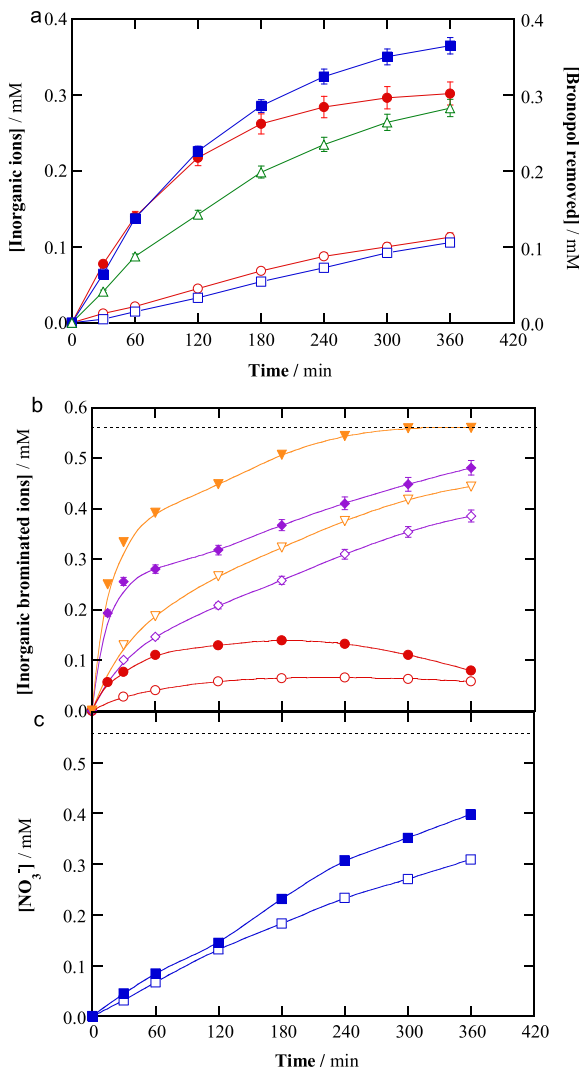


Fig. 6. (a) Evolution of the concentration of (\bigcirc , \bullet) Br^- and (\square , \blacksquare) NO_3^- released and (\triangle) bronopol removed during the (\bigcirc , \square , \triangle) $\text{EO-H}_2\text{O}_2$ and (\bullet , \blacksquare) PEF (with 0.50 mM Fe^{2+}) treatments of 2.5 L of 0.56 mM (20 mg L^{-1} TOC) bronopol in $0.020\text{ M Na}_2\text{SO}_4$ at $\text{pH } 3.0$ and $35\text{ }^\circ\text{C}$ using a RuO_2 -based anode and (Co, S, P)-modified MWCNTs air-diffusion cathode at $j = 20\text{ mA cm}^{-2}$ and liquid flow rate of 180 L h^{-1} . (b) Evolution of the concentration of (\bigcirc , \bullet) Br^- , (∇ , \blacktriangledown) BrO_3^- , (∇ , \blacktriangledown) sum of $\text{Br}^- + \text{BrO}_3^-$ and (c) (\square , \blacksquare) NO_3^- released during the (\bigcirc , \square , ∇ , \blacktriangledown) $\text{EO-H}_2\text{O}_2$ and (\bullet , \blacksquare , \blacktriangledown) PEF treatments under the same conditions, but using a BDD anode.

led to a pseudo-first-order kinetics with $k_{\text{app}} = 0.007\text{ min}^{-1}$ (Fig. 4b). In contrast, the anode had a less significant role in PEF, showing almost no difference in bronopol removal due to the superior contribution of 'OH in the bulk (Fig. 4a). However, BDD exhibited a positive effect as for TOC abatement, since the reaction of BDD('OH) with very stable by-products and their Fe(III) complexes favored the quicker mineralization, attaining 91% instead of 77% (Fig. 4c).

3.3. Detection of final carboxylic acids and fate of inorganic ions

The intensive action of 'OH and M('OH) on aromatic and aliphatic pollutants usually causes the accumulation of short-chain aliphatic carboxylic acids, which account for the high refractoriness of solution TOC during the last stages of EAOPs. In the present work, formic acid was identified as the main degradation by-product by ion-exclusion HPLC, in agreement with that observed in our previous study [52].

Fig. 5a shows the concentration profiles of this acid in the three EAOPs tested, with the RuO_2 -based anode and catalyzed cathode, at 40 mA cm^{-2} . The concentration gradually increased in $\text{EO-H}_2\text{O}_2$ and PEF, attaining $10\text{--}13\text{ mg L}^{-1}$ at 360 min , whereas it was completely destroyed in PEF, thus justifying the larger TOC removal attained in it (Fig. 3c). Fig. S6a highlights a difference between solution TOC and (bronopol + formic acid) equivalent TOC at each time, which can be related with the accumulation of unidentified organic by-products. Fig. 5b evidences that the treatment of more concentrated bronopol solutions by PEF involved a larger accumulation of formic acid, which was very refractory and remained in the final solutions, in agreement with the large TOC amount at 360 min shown in Fig. S6b. Fig. S6b informs about the existence of unidentified by-products.

Several electrolyses were performed with the catalyzed cathode to determine the inorganic ions released from the heteroatoms contained in solutions with 0.56 mM bronopol. Fig. 6a shows the time course of ions in $\text{EO-H}_2\text{O}_2$ and PEF with a RuO_2 -based anode. In the former treatment, 0.11 mM Br^- and 0.11 mM NO_3^- were accumulated at 360 min , along with half of the initial concentration of bronopol, whereas 0.30 mM Br^- and 0.36 mM NO_3^- were released in PEF. This means that some brominated and nitrogenated molecules were also formed, accounting for by the undetected Br and N content, since neither BrO_3^- nor NO_2^- appeared in the chromatograms and less than 1 mg L^{-1} NH_4^+ was found. Based on the conclusions from Fig. S6a and S6b, the undetected molecules corresponded to organic compounds, as for example bromonitromethane [52]. Fig. 6b and c illustrate the results obtained for brominated and nitrogenated ions by analogous trials with BDD anode, respectively. Also in these cases, some organic by-products containing Br and N were plausibly formed, being the main difference the progressive transformation of Br^- into BrO_3^- upon attack of 'OH and M('OH) [5].

3.4. Solar photoelectro-Fenton treatment

Since PEF showed the best performance among all EAOPs, the possibility of using sunlight as an inexpensive irradiation source was explored. Fig. 7 shows the performance of SPEF treatments of 0.28 mM bronopol solutions with either a RuO_2 -based or BDD anode at $j = 40\text{ mA cm}^{-2}$. Total bronopol removal was achieved at 360 and 300 min using the RuO_2 -based anode and the uncatalyzed and catalyzed cathode, respectively (Fig. 7a). This confirms the enhanced degradation with the Co-based cathode, as well as the aimed superiority of SPEF over PEF (Fig. 2a) thanks to the greater photon flux and the contribution of visible photons of sunlight. The corresponding k_{app} values were 0.012 and 0.016 min^{-1} (Fig. 7b). These findings were verified with the BDD anode, which allowed the complete destruction after 300 and 210 min (k_{app} of 0.018 and 0.021 min^{-1}), quicker than PEF (Fig. 4a). SPEF treatment with the BDD anode and catalyzed air-diffusion cathode was the best among all EAOPs, yielding a greater mineralization of 94% at 360 min (Fig. 7c) as compared to PEF (Fig. 4c) and giving rise to the highest MCE values of this study (Fig. 7d). The replacement of BDD by the less expensive RuO_2 -based anode led to a TOC removal of 88%, exhibiting a lower energy consumption (Fig. 7e) due to the decrease in E_{cell} .

4. Conclusions

This work has demonstrated that Co-based air-diffusion cathodes enhance the electrocatalytic H_2O_2 production as compared to uncatalyzed ones, reaching up to 100% current efficiency at low j . These cathodes showed a good stability during prolonged electrolyses, showing a small Co release into treated solutions. The great H_2O_2 generation served to produce 'OH from Fenton's reaction in the presence of 0.50 mM Fe^{2+} . As a result, complete removal of bronopol with

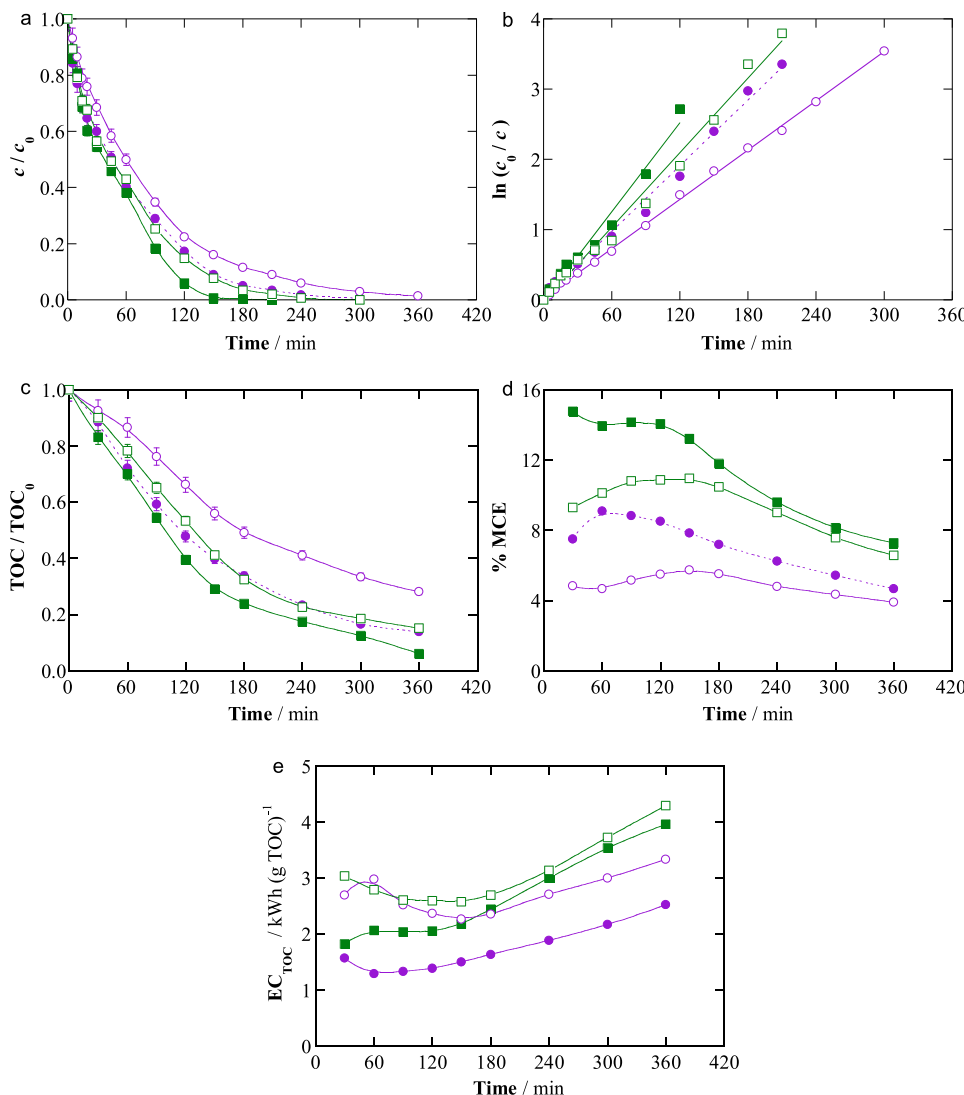


Fig. 7. (a) Normalized bronopol concentration removal vs. time and (b) corresponding pseudo-first-order kinetic analysis, (c) normalized TOC decay with electrolysis time and corresponding (d) mineralization current efficiency and (e) specific energy consumption per unit TOC mass during the SPEF treatment of 2.5 L of 0.28 mM bronopol solutions in 0.050 M Na_2SO_4 with 0.50 mM Fe^{2+} at pH 3.0 and 35 °C using a (○, ●) RuO_2 -based or (□, ■) BDD anode and (○, □) uncatalyzed or (●, ■) (Co, S, P)-modified MWCNTs air-diffusion cathode at $j = 40 \text{ mA cm}^{-2}$ and liquid flow rate of 180 L h^{-1} .

a large percentage of mineralization was achieved, with performance increasing in the sequence: $\text{EO-H}_2\text{O}_2 < \text{EF} < \text{PEF} < \text{SPEF}$. BDD was superior to the RuO_2 -based anode due to the higher oxidation power of $\text{BDD}(\text{OH})$ as compared to $\text{RuO}_2(\text{OH})$. Bronopol was mainly transformed into formic acid as final by-product, although the formation of some other organic intermediate with Br and N atoms was also deduced from the accumulation profiles of Br^- , BrO_3^- and NO_3^- ions.

Acknowledgements

The authors thank financial support from project CTQ2016-78616-R (AEI/FEDER, EU) and PhD scholarship awarded to Z. Ye (State Scholarship Fund, CSC, China). This Special Issue is dedicated to honor the retirement of Prof. César Pulgarin at the Swiss Federal Institute of Technology (EPFL, Switzerland), a key figure in the area of Catalytic Advanced Oxidation Processes.

Appendix A. Supplementary data

Supplementary material related to this article can be found, in the online version, at doi:<https://doi.org/10.1016/j.apcatb.2019.01.029>.

References

- [1] J.M. Campos-Martín, G. Blanco-Brieva, J.L. Fierro, *Angew. Chem. Int. Ed.* **45** (2006) 6962–6984.
- [2] ReportLinker, Future of Global Hydrogen Peroxide Market to 2025- Growth Opportunities, Competition, Trends and Outlook of Hydrogen Peroxide Across Applications and Regions Report, (2018) (accessed 24 September 2018), <https://www.reportlinker.com/p05505747/Future-of-Global-Hydrogen-Peroxide-Market-to-Growth-Opportunities-Competition-Trends-and-Outlook-of-Hydrogen-Peroxide-Across-Applications-and-Regions-Report.html>.
- [3] S. Yang, A. Verdaguera-Casadevall, L. Arnarson, L. Silvioli, V. Čolić, R. Frydendal, J. Rossmeisl, Ib Chorkendorff, I.E.L. Stephens, *ACS Catal.* **8** (2018) 4064–4081.
- [4] M.A. Oturan, J.-J. Aaron, *Crit. Rev. Environ. Sci. Technol.* **44** (2014) 2577–2641.
- [5] I. Sirés, E. Brillas, M.A. Oturan, M.A. Rodrigo, M. Panizza, *Environ. Sci. Pollut. Res.* **21** (2014) 8336–8367.
- [6] E. Brillas, I. Sirés, M.A. Oturan, *Chem. Rev.* **109** (2009) 6570–6631.
- [7] E. Brillas, *J. Braz. Chem. Soc.* **25** (2014) 393–417.
- [8] M. Zhou, M.A. Oturan, I. Sirés, *Electro-Fenton Process – New Trends and Scale-Up, The Handbook of Environmental Chemistry vol. 61*, Springer Nature, Singapore, 2018.
- [9] A. Ashgar, A.A.A. Raman, W.M.A.W. Daud, M. Ahmad, S.U.B.M. Zain, *J. Taiwan Inst. Chem. Eng.* **76** (2017) 89–100.
- [10] M. Panizza, M.A. Oturan, *Electrochim. Acta* **56** (2011) 7084–7087.
- [11] G. Coria, T. Pérez, I. Sirés, J.L. Nava, *J. Electroanal. Chem.* **757** (2015) 225–229.
- [12] O. Ganzenko, N. Oturan, I. Sirés, D. Huguenot, E.D. van Hullebusch, G. Esposito, M.A. Oturan, *Environ. Chem. Lett.* **16** (2018) 281–286.
- [13] H.C. Arredondo Valdez, G. García Jiménez, S. Gutiérrez Granados, C. Ponce de

León, Chemosphere 89 (2012) 1195–1201.

[14] A. Thiam, I. Sirés, F. Centellas, P.L. Cabot, E. Brillas, Chemosphere 136 (2015) 1–8.

[15] X. Yu, M. Zhou, G. Ren, L. Ma, Chem. Eng. J. 263 (2015) 92–100.

[16] A. Galia, S. Lanzalaco, M.A. Sabatino, C. Dispenza, O. Scialdone, I. Sirés, Electrochim. Commun. 62 (2016) 64–68.

[17] Y. Lu, G. Liu, H. Luo, R. Zhang, Electrochim. Acta 248 (2017) 29–36.

[18] G. Coria, T. Pérez, I. Sirés, E. Brillas, J.L. Nava, Chemosphere 198 (2018) 174–181.

[19] T. Pérez, G. Coria, I. Sirés, J.L. Nava, A.R. Uribe, J. Electroanal. Chem. 812 (2018) 54–58.

[20] J.F. Pérez, J. Llanos, C. Sáez, C. López, P. Cañizares, M.A. Rodrigo, Electrochim. Commun. 71 (2016) 65–68.

[21] O. Scialdone, A. Galia, C. Gattuso, S. Sabatino, B. Schiavo, Electrochim. Acta 182 (2015) 775–780.

[22] K.V. Plakas, A.J. Karabelas, S.D. Sklari, V.T. Zaspalis, Ind. Eng. Chem. Res. 52 (2013) 13948–13956.

[23] H. Roth, Y. Gendel, P. Buzatu, O. David, M. Wessling, J. Hazard. Mater. 307 (2016) 1–6.

[24] F. Yu, Y. Chen, H. Ma, New J. Chem. 42 (2018) 4485–4494.

[25] T.X.H. Le, M. Bechelany, S. Lacour, N. Oturan, M.A. Oturan, M. Cretin, Carbon 94 (2015) 1003–1011.

[26] E. Mousset, Z. Wang, J. Hammaker, O. Lefebvre, Electrochim. Acta 214 (2016) 217–230.

[27] W. Yang, M. Zhou, J. Cai, L. Liang, G. Ren, L. Jiang, J. Mater. Chem. A Mater. Energy Sustain. 5 (2017) 8070–8080.

[28] J.C. Murillo-Sierra, I. Sirés, E. Brillas, E.J. Ruiz-Ruiz, A. Hernández-Ramírez, Chemosphere 192 (2018) 225–233.

[29] G.R. Agladze, G.S. Tsurtsumia, B.-I. Jung, J.-S. Kim, G. Gorelishvili, J. Appl. Electrochem. 37 (2007) 375–383.

[30] G. Coria, I. Sirés, E. Brillas, J.L. Nava, Chem. Eng. J. 304 (2016) 817–825.

[31] A. Thiam, R. Salazar, E. Brillas, I. Sirés, Chem. Eng. J. 335 (2018) 133–144.

[32] A. Verdaguera-Casadevall, D. Deiana, M. Karamad, S. Siahrostami, P. Malacrida, T.W. Hansen, J. Rossmeisl, I. Chorkendorff, I.E.L. Stephens, Nano Lett. 14 (2014) 1603–1608.

[33] R.M. Félix-Navarro, M. Beltrán-Gastélum, M.I. Salazar-Gastélum, C. Silva-Carrillo, E.A. Reynoso-Soto, S. Pérez-Sicarios, S.W. Lin, F. Paraguay-Delgado, G. Alonso-Núñez, J. Nanopart. Res. 15 (1802) (2019) 11pages.

[34] E.C. Paz, L.R. Aveiro, V.S. Pinheiro, F.M. Souza, V.B. Lima, F.L. Silva, P. Hammer, M.R.V. Lanza, M.C.S. Santos, Appl. Catal. B: Environ. 232 (2018) 436–445.

[35] C. Ridruejo, F. Alcaide, G. Álvarez, E. Brillas, I. Sirés, J. Electroanal. Chem. 808 (2018) 364–371.

[36] L. Liang, Y. An, M. Zhou, F. Yu, M. Liu, G. Ren, J. Environ. Chem. Eng. 4 (2016) 4400–4408.

[37] W.R.P. Barros, P.C. Franco, J.R. Steter, R.S. Rocha, M.R.V. Lanza, J. Electroanal. Chem. 722–723 (2014) 46–53.

[38] C. Espinoza, J. Romero, L. Villegas, L. Cornejo-Ponce, R. Salazar, J. Hazard. Mater. 319 (2016) 24–33.

[39] F. Gozzi, I. Sirés, A. Thiam, S.C. de Oliveira, A. Machulek Jr., E. Brillas, Chem. Eng. J. 310 (2017) 503–513.

[40] T. Pérez, I. Sirés, E. Brillas, J.L. Nava, Electrochim. Acta 228 (2017) 45–56.

[41] J.R. Steter, E. Brillas, I. Sirés, Appl. Catal. B: Environ. 224 (2018) 410–418.

[42] I. Salmerón, K. Plakas, I. Sirés, I. Oller, M.I. Maldonado, A.J. Karabelas, S. Malato, Appl. Catal. B: Environ. 242 (2019) 327–336.

[43] B. Marselli, J. García-Gómez, P.A. Michaud, M.A. Rodrigo, C. Cominellis, J. Electrochem. Soc. 150 (2003) D79–D83.

[44] M. Panizza, G. Cerisola, Chem. Rev. 109 (2009) 6541–6569.

[45] C.A. Martínez-Huiti, M. Panizza, Curr. Opin. Electrochem. 11 (2018) 62–71.

[46] M.A. Pastor-Nieto, F. Alcántara-Nicolás, V. Melgar-Molero, R. Pérez-Mesonero, A. Vergara-Sánchez, A. Martín-Fuentes, P. González-Muñoz, E. de Eusebio-Murillo, Actas Dermosifiliogr. 108 (2017) 758–770.

[47] M. Kireche, J.-L. Peiffer, D. Antonios, I. Fabre, E. Giménez-Arnau, M. Pallardó, J.-P. Lepoittevin, J.-C. Ourlin, Chem. Res. Toxicol. 24 (2011) 2115–2128.

[48] V. Tornero, G. Hanke, Marine Pollut. Bull. 112 (1–2) (2016) 17–38.

[49] C. Dye, M. Schlach, J. Green, M. Remberger, L. Kaj, A. Palm, Bronopol, resorcinol, *m*-cresol and triclosan in the nordic environment, in: B. Bürgel Mogenesen, M.J.P.H. Dam, J.A.S.S. Mannio, O.B.H. Glesne, K. Suomalainen (Eds.), Thema North, Nordic Screen Reports, Nordic Council of Ministers, Copenhagen, 2007.

[50] R. Kallenborn, E. Brorström-Lundén, L.O. Reiersen, S. Wilson, Environ. Sci. Pollut. Res. 25 (2018) 33001–33013.

[51] M. Matczuk, N. Obarski, M. Mojski, Int. J. Cosmet. Sci. 34 (2012) 451–457.

[52] E. Bocos, E. Brillas, M.A. Sanromán, I. Sirés, Environ. Sci. Technol. 50 (2016) 7679–7686.

[53] J. Dong, D. Li, Z. Peng, Y. Zhou, J. Solid State Electrochem. 12 (2008) 171–174.

[54] G. Álvarez, F. Alcaide, P.L. Cabot, M.J. Lázaro, E. Pastor, J. Solla-Gullón, Int. J. Hydrog. Energy 37 (2012) 393–404.

[55] R.F. Pupo Nogueira, M.C. Oliveira, W.C. Paterlini, Talanta 66 (2005) 86–91.